Norbornadiene/Quadricyclane System in the Spotlight: The Role of Rydberg States and Dynamic Electronic Correlation in a Solar-Thermal Building Block

Federico Coppola, Martina Nucci, Marco Marazzi, Dario Rocca, Mariachiara Pastore

Norbornadiene/Quadricyclane System in the Spotlight: The Role of Rydberg States and Dynamic Electronic Correlation in a Solar-Thermal Building Block

Federico Coppola,[a] Martina Nucci,[b] Marco Marazzi,*[b,c] Dario Rocca,[a] Mariachiara Pastore*[a]

Dedication (optional, leave blank if no dedication is required)

In this contribution, we studied the photophysics and photochemistry of an archetypal molecular switch in terms of solar energy storage and release. In detail, we characterized the valence and Rydberg states of norbornadiene (NBD) and quadricyclane (QC) by means of CASPT2//CASSCF theory level, finding a good agreement of the calculated vertical excitation energies with the experimental counterparts. The NBD↔QC thermal and photochemical valence isomerization [2π+2π] reactions have been addressed and investigated. Low energy crossing points between excited states were identified for both the NBD↔QC photochemical reactions, through the calculation of minimum energy paths which revealed that the photochemistry is ruled by the deformation of two coupled reaction coordinates. Such coordinates were also used to build potential energy surfaces through relaxed energy scans with the goal of building a simplified, still accurate, model system able to catch the NBD↔QC photorelaxation. Also, the S_1/S_0 respective conical intersection were characterized and related to the reaction quantum yield. Interestingly, we found that reverse photoisomerization from QC to the NBD progenitor could in principle occur by direct excitation of σ-3_s and σ-3_p Rydberg excited states in the UV spectral range. In both NBD and QC photoreactivity, the doubly excited valence state has shown to play a crucial role for reaching crossing points leading to nonadiabatic population transfers.

[a] Dr. Federico Coppola, Prof. Dario Rocca, Dr. Mariachiara Pastore*
Laboratoire de Physique et Chimie Théoriques (LPCT), Université de Lorraine & CNRS, UMR 7019, F-54000 Nancy, France
E-mail: mariachiara.pastore@univ-lorraine.fr

[b] Martina Nucci, Prof. Marco Marazzi*
Universidad de Alcalá, Departamento de Química Analítica, Química Física e Ingeniería Química, Grupo de Reactividad y Estructura Molecular (RESMOL), Alcalá de Henares, Madrid, Spain
E-mail: marco.marazzi@uah.es

[c] Universidad de Alcalá, Instituto de Investigación Química "Andrés M. del Río" (IQAR), Alcalá de Henares, Madrid, Spain

Introduction

During the last decades, a fervent research activity has been focused on the development of photovoltaics (PVs) for conversion of solar energy into electricity.[1] Nevertheless, to serve as a primary energy source, solar energy technologies need to be coupled with expensive battery banks of considerable size. An alternative solution to the problem of energy storage (and *a posteriori* release) is constituted by the use of specifically designed molecules that can be photocharged, thus storing part of the photon energy through a rearrangement of their chemical bonds and geometrical conformation.[2] In this context, it is known that molecular photoswitches can undergo a closed cycle, reversibly storing energy upon light irradiation (through a photochemical reaction converting a stable isomer into a higher energy one) and releasing it, on demand, by a second thermal or catalytic reaction, thus combining energy harvest and release in a single system. Such molecules are therefore named molecular solar thermal (MOST)[3] systems or solar thermal fuels (STF).[4,5] To be of technological relevance, photochromic systems for targeted MOST applications must fulfill several requirements:[6–8] i) absorbance of the stable isomer within the solar spectrum; ii) no optical activity of the metastable high-energy isomer; iii) low molecular weight and possibly high energy difference between the two isomers to have high energy storage density; iv) a high energy barrier for the back reaction to ensure long-term energy storage; v) good cyclability; vi) absence of side reactions and vii) cost-competitiveness. It is therefore evident that to match all these properties, the molecular design of efficient MOSTs is extremely challenging since, as often occurs, optimizing one property may cause deterioration of another one.[9] Therefore, it is recently emerging the necessity of rationalizing the mechanism through theoretical calculations. Several functionalized photoswitches (in solution[10] or embedded in polymer matrices[11–13]) have proved their potentiality to serve as MOSTs, such as stilbenes[14,15], anthracenes[16,17], azobenzenes[18–20], dihydroazulenes[21],norbornadienes[8,12,22–30] and fulvalene ruthenium[31–33] compounds.

The unsubstituted norbornadiene (NBD)/quadricyclane (QC) couple, being the focus of the present work (see Figure 1), is of particular interest because of its low molecular weight, appreciable energy storage (146 kJ mol^{-1}), and relatively high energy barrier (96 kJ mol^{-1}) for the thermal back-conversion of QC to the parent form NBD.[34–36] More-

over, the half-life of QC is of the order of hundreds of years at room temperature,[37,38] guaranteeing that the stored energy can be released on demand by adding a proper catalyst. On the flip side, NBD absorbs in the UV region, at 267 nm, and this represents its main drawback, as the overlap with the maximum of the solar spectral irradiance, at $\sim$ 590 nm, is narrow. Such limitation can be handled differently, applying intense UV light to prepare the QC photoproduct with satisfactory yields, using photosensitizers as acetophenone or Michler's ketones,[22,39,40] or considering different substitution patterns, in order to selectively introduce a bathochromic shift in the NBD absorption spectrum.[41]

The relevant photochemistry occurs on the singlet potential energy surface manifold, and a conical intersection between the ground state and first singlet excited state is usually considered as the only relevant structure determining the fate of the whole photoreactivity. Nevertheless, the literature lacks a detailed description of the full mechanism depicting all events from NBD absorption to QC production, and the eventual (but usually neglected) reverse photoreaction. The study of NBD→QC photodynamics and related

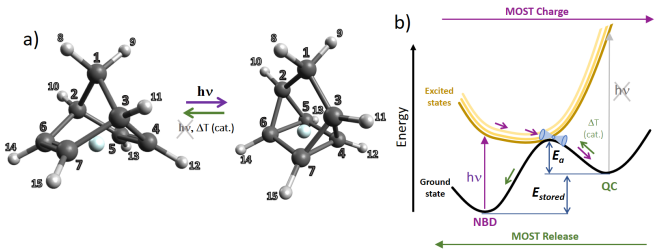

Figure 1. Reactivity of the norbornadiene/quadricyclane system from a) structural and b) energy points of view, highlighting the MOST charge and release steps, in violet and green, respectively. Reverse photoisomerization is also depicted as undesired event. IUPAC name: bicyclo[2.2.1]hepta-2,5-diene for NBD and tetracyclo[3.2.0.$0^{2,7}$.$0^{4,6}$]heptane for QC. Atom color code: gray=carbon, white=hydrogen, light blue=center of charge.

kinetics was reported by Fuß et al.[42] in 2002: upon photoexcitation at 200 nm, two states were found to be simultaneously populated, namely the second π-π^* state and a 3*s* Rydberg state, hence evidencing the necessity to include low-energy Rydberg states in the description of the photoprocess. All the transitions from one surface to another, occurring on the *sub-ps* timescale, were rationalized considering the presence of easily accessible conical intersections (CI) between Rydberg and valence states. On the basis of symmetry considerations it was predicted that the conical intersection with the ground state (S_1/S_0) could be reached following a rhombic distortion. With a theoretical approach, Antol[43] also highlights the key role of low-energy Rydberg states and identifies the main reaction coordinates showing that the NBD→QC photoprocess has negligible barriers, thus occurring on ultrafast time scales. Recently,[44] the same reactivity was studied by quantum dynamics. Nevertheless, this study only relying on the CASSCF approximation, neglects the dynamic electronic correlation effects, that may be of fundamental importance to get a reliable description of both energetic and kinetic aspects. On the other hand, the NBD→QC photoreactivity has been poorly investigated, while thermal cycloreversion, yielding to the energy release step, is well known.[45] Nonetheless, the QC photochemistry needs also to be addressed in detail, in order to prevent undesired QC→NBD photoreversion. By chemical intuition, such possibility is usually ruled out due to the fact that QC has no π orbitals, and thus it should not be considered as a chromophore (Figure 1a). Nevertheless, this simplified picture takes into account only valence states, while QC→NBD photoisomerization dynamics point toward two close in energy Rydberg states as the ones playing a role in restoring the NBD isomer.[46] More in detail, QC undergoes reverse photoisomerization on the 3*s* Rydberg surface, while the 3*p* state is trapped in a minimum. Nevertheless, higher-energy Rydberg states could also play a role and, to the best of our knowledge, the QC→NBD eventual photochemical path, together with possible side photoreactions, has been never investigated.

It appears, thus, clear that a reliable characterization of the NBD↔QC reactivity is a complicated task, that would greatly benefit from the results of theoretical calculations addressing the possible photoreaction pathways by considering both valence and Rydberg excited states and capable to properly include static and dynamic electronic correlation. Here, we tackle this challenge by performing extensive multireference perturbation theory calculations (CASPT2)[47] on the the low-lying valence and Rydberg excited states of NBD/QC.

Results and Discussion

The absorption spectrum of NBD

The experimental spectrum of NBD exhibits several sharp bands overlapped to three structureless signatures in the 240-170 nm region. According to the selection rules and symmetry considerations, it was possible to discriminate the Rydberg transitions (at 5.85, 6.40, 6.60 and 6.91 eV) from the two valence states peaked at 6.00 and 6.70 eV, respectively.[47] CASPT2//CASSCF calculations allowed for a detailed interpretation of the experimental spectrum by providing information on the nature of the bright electronic transitions composing each absorption band. The first, optically forbidden, valence state with a HOMO-LUMO character (1^1A_2, π_2-π_3^*) was calculated at 5.28 eV, while a weak valence state of $^1B_2$ symmetry with a HOMO-1-LUMO and HOMO-LUMO+1 mixed character (π_1-π_3^*, π_2-π_4^*) was predicted at 6.20 eV. The latter assignment was, however, less certain due to the presence of narrowly spaced bands overlapped on a much broader background in the same spectral region. To solve this specific uncertainty, McDiarmid and co-workers[48] experimentally refined the assignment of electronic states in the 198-225 nm spectral region, attributing the peak at 5.61 eV to the 3*s* Rydberg transition and the subsequent band, at 5.74 eV, to the valence state at issue. The most intense transition in the NBD spectrum populates a valence excited state (2^1B_2, $\pi_{1(2)}$-$\pi_{3(4)}^*$) appearing at 6.48 eV. Above 7.00 eV, the last two valence states are very close in energy, a singly excited optically forbidden band ($^1A_2$, π_1-π_4^*) at 7.36 eV and a weak double excited state ($^1A_1$, $(\pi_2$-$\pi_3^*)_2$) at 7.49 eV. Two $3s-3p-3d$ Rydberg series of NBD, respectively originated out of the HOMO ($^1B_1$) and HOMO-1 ($^1A_1$) orbitals, appear in the absorption spectrum between the valence states. The first series ($\pi_2\rightarrow$ 3*s*, 3*p*, 3*d*) is computed at 5.73, 6.23 and 6.70 eV, respectively, followed by the $\pi_1\rightarrow$ 3*s*, 3*p*, 3*d* Rydberg transitions at 6.67, 6.94 and 7.51 eV, respectively. In both cases the $\pi_{1(2)}\rightarrow$ 3*s* are the only slightly bright states.

Furthermore, in a previous experimental study,[49] the optically dark valence state was assigned at 5.23 eV, while the band peaking at 5.95 eV was assigned to a π_2-3s Rydberg transition, making uncertain the assignment of the close-by second valence state. Finally, the band around 6.85 eV was tentatively attributed to the π_1-3s Rydberg transition, with the brightest transition at almost the same energy (6.88 eV). More recently, the low-lying valence excited states of NBD have been characterized (results are summarized in Table 1 in ESI) by means of high level *ab-initio* calculations within multireference approaches (CASSCF[50], CASPT2, Coupled Cluster[51] and NEVPT2[52] methods) by evaluating also the effect of different basis sets[53,54] on vertical excitation energy and their electronic properties.

Table 1 collects the CASSCF and CASPT2 vertical excitations energies for the NBD molecule calculated in this work, along with the assignment of the valence/Rydberg nature of the electronic excited states. The expectation values of second Cartesian moments ($\langle \mathbf{x}^2 \rangle$, $\langle \mathbf{y}^2 \rangle$, $\langle \mathbf{z}^2 \rangle$) have been used as a further confirmation of the pure or mixed valence and Rydberg nature of the states. The calculated vertical excitation energy to the first electronic state is 6.57/6.34 eV at CASSCF/(SS)-CASPT2 level and corresponds to the optically bright π_2-3s Rydberg transition. The pure Rydberg character of this state is confirmed by the rather large expectation values of the Cartesian second moments as well as by the fact that application of the multi state (MS)-CASPT2 correction does not yield to significant change in the excitation energy, being calculated at 6.31 eV. The second electronic transition at CASSCF level, V_1, is predicted at 6.75 eV, it is dipole-forbidden and shows a mixed valence (HOMO→LUMO)-Rydberg (HOMO→3p$_y$) character. As expected, dynamic electronic correlation effects have a remarkable contribution on this state, which becomes the lowest-energy excited state upon MS-CASPT2 correction, with an excitation energy of 4.83 eV. This value appears to be slightly underestimated with respect to the experimental assignment at 5.25 eV[42], as well as significantly lower than the CC3 value (5.64 eV) calculated in Ref. 51 and reported in Table S1. Due to the mixing with Rydberg states, it is, however, difficult to evaluate the accuracy of our estimation by direct comparison with the previous CC3/TZVP calculations, that do not properly take into account the presence of low-lying Rydberg states. It is worth mentioning, however, that, for single reference excited states, CC3 vertical transition energies have been shown to be quite closer to experiments with respect to those obtained with MRPT2 approximations.[55] On its side, the π_2-3p$_y$ state, calculated at 8.53 eV by CASSCF, is over-corrected at 6.75 eV by SS-CASPT2, due to its partial valence character, and finally located at 7.38 eV once the multistate correction is applied. As shown in Table 1 by the differences between the SS- and MS-CASPT2 results, these are the only two states that are significantly mixed in the CASSCF wavefunction. An almost dark doubly excited valence state - $V_2(\pi_2\text{-}\pi_3^*)_2$ - is present at 7.66 eV (CASSCF) and involves the promotion of two electrons from the HOMO to the LUMO. A small correlation energy contribution (ca. 0.2 eV) is gained upon CASPT2 correction. In increasing energy order, the principal electronic configuration describing the $S_0 \rightarrow S_4$ vertical transition (7.80 eV at CASSCF level) involves the promotion of an electron from the HOMO (π_2) to a diffuse Rydberg orbital (3d$_{z^2}$), as showed by a remarkably high $\langle \mathbf{z}^2 \rangle$ component compared with those of the ground state. This almost dark vertical transition is slightly stabilized at CASPT2 level by about 0.4 eV. The π_1-3d$_{z^2}$ state, being the fifth excited state at CASSCF level, is among the brightest states of NBD (f_{OSC}: $1.55 \cdot 10^{-1}$). The CASSCF vertical excitation energy of 8.01 eV is significantly decreased when the CASPT2 correction is applied, yielding to 7.37 and 7.33 eV by single- and multi-state CASPT2, respectively. The singlet state at 8.35 eV has a valence character (V_3), it is dominated by a π_1-π_3* configuration and is also predicted to be optically bright. Moreover, a large second order perturbation correction places the vertical excitation of this state at 6.81 eV, just above the dark V1 and the bright RYD π_2-3s states, and in quite good agreement with the experimental assignment at 6.65-6.70 eV[47]. A value of 7.10 eV has been obtained by Thiel and co-workers[52] by using PC-NEVPT2 with a TZVP basis set, while CC3/TZVP predicts this excitation at 7.64 eV. Finally the S_8 state is calculated to lie at 9.18 eV above the ground state by CASSCF and at about 8.40 eV by CASPT2. The second Cartesian moment along the z-axis highlights its Rydberg character, mainly dominated by the π_1-3s configuration. The computed oscillator strength value is similar to that of the analogous π_2-3s lower energy Rydberg state. As can be inferred by comparing the present results with those reported in Table 1 in ESI, the calculated excitation energy of the dark valence state is particularly in good agreement with the value calculated within the same perturbative approach when using a Dunning-type basis set as well as with the NEVPT2 treatment in both strongly- and partially-contracted variants, and similarly a good agreement is also found for the bright valence state. Few results are present in previous works concerning the doubly excited valence state, which is, however, calculated at ca. 7.5 eV at CASPT2 level, regardless of the employed basis set. On the other hand, for the Rydberg excitations, which have been not adequately taken into account in previous works, the agreement slightly worsens, also due to the different choice of the active spaces and/or the quality of the reference wave function and basis set.

The absorption spectrum of QC

To the best of our knowledge, only a few studies have appeared in the literature on the electronic structure and optical properties of the highly-strained quadricyclane photoproduct. The photoelectron spectrum was recorded in the early seventies[56,57] and four distinct bands were measured in the 8-11 eV energy range. This is consistent with the fact that, coherently with MOST applications, light irradiation of the higher energy isomer QC should not lead to any appreciable photochemistry. From the experimental investigation of the QC→NBD photoisomerization dynamics by Rudakov and Weber,[46] the 3s and 3p$_{x,y}$ Rydberg states were nevertheless observed at 2.88, 2.29 and 2.24 eV respectively, hence indicating also for QC the necessity to include Rydberg states in the calculations through appropriate basis set augmentation.

Indeed, we found a dense manifold of Rydberg-type excited states ranging from ca. 6 to 9 eV (210 - 140 nm), hence in principle partially overlapping with the NBD absorption window. However, differently from NBD, no pure valence states are observed (see Table 2). The average orbital coefficients are severely mixed and a clear identification is far from an easy task. In Table 2, under *Principal configuration*, we report in gray the less relevant, but still non-negligible, orbital contributions. The second Cartesian moments com-

Table 1. NBD absorption spectrum values: principal configuration for the first nine singlet states (S_n) and vertical excitation energies (eV) at CASSCF, SS- and MS-CASPT2 levels. The expectation values of second Cartesian moments ($\langle \mathbf{x}^2 \rangle$,$\langle \mathbf{y}^2 \rangle$,$\langle \mathbf{z}^2 \rangle$ in au^2) are given at CASSCF level. Oscillator strengths (f_{OSC}, dimensionless) are computed at CASSCF and MS-CASPT2 level.

E. S.	Configuration	CASSCF	f_{OSC}	$\langle \mathbf{x}^2 \rangle$	$\langle \mathbf{y}^2 \rangle$	$\langle \mathbf{z}^2 \rangle$	Configuration	SS-CASPT2	Configuration	MS-CASPT2	f_{OSC}
S_0	G.S. π_1-π_2	0.00	–	-31.07	-26.63	-30.93	G.S. π_1-π_2	0.00	G.S. π_1-π_2	0.00	–
S_1	RYD π_2 -3s	6.57	$4.04*10^{-2}$	-35.56	-40.57	-48.50	V_1 π_2-π_3*	5.45	V_1 π_2-π_3*	4.83	–
S_2	V_1 π_2-π_3*	6.75	–	-29.41	-38.16	-38.79	RYD π_2 -3s	6.34	RYD π_2 -3s	6.31	$2.98*10^{-2}$
S_3	$V_2(\pi_2$-π_3*$)_2$	7.66	$1.12*10^{-4}$	-30.20	-30.57	-31.99	RYD π_2-3p$_y$	6.75	V_3 π_1-π_3	6.81	$1.38*10^{-1}$
S_4	RYD π_2-3d$_{z^2}$	7.80	$1.80*10^{-4}$	-32.24	-36.56	-53.77	V_3 π_1-π_3*	6.81	RYD π_1-3d$_{z^2}$	7.33	$1.43*10^{-1}$
S_5	RYD π_1-3d$_{z^2}$	8.01	$1.55*10^{-1}$	-37.29	-41.00	-46.62	RYD π_2-3d$_{z^2}$	7.36	RYD π_2-3p$_y$	7.38	–
S_6	V_3 π_1-π_3*	8.35	$1.54*10^{-1}$	-30.86	-40.45	-39.55	RYD π_1-3d$_{z^2}$	7.37	RYD π_2-3d$_{z^2}$	7.40	$1.57*10^{-4}$
S_7	RYD π_2-3p$_y$	8.53	–	-32.60	-40.30	-36.45	$V_2(\pi_2$-π_3*$)_2$	7.46	$V_2(\pi_2$-π_3*$)_2$	7.47	$1.08*10^{-4}$
S_8	RYD π_1-3s	9.18	$2.62*10^{-2}$	-32.86	-35.56	-53.93	RYD π_1-3s	8.40	RYD π_1-3s	8.44	$2.41*10^{-2}$

puted at CASSCF level are consistent with the typical spatial extension of Rydberg-type orbitals.

The first electronic excitation, predicted at about 5.70 eV by both CASSCF and CASPT2, is a dark state involving the promotion of an electron from the HOMO to a mixed 3s, 3p$_y$ Rydberg-type orbital. At 6.31 eV a dipole-forbidden σ_2-3p$_z$ Rydberg state is computed at CASSCF level; dynamic electronic correlation slightly decreases its excitation energy to $\simeq$ 6.0 eV. At CASSCF level, a pair of weakly bright electronic transitions, very similar in nature despite the different orbital contributions, follows, at 6.64 and 6.78 eV. These states are slightly stabilized (about 6.50 and 6.69 eV) by CASPT2 correction. The fifth singlet state in the CASSCF calculation is the σ_2-3d$_{z^2}$ state, computed at 7.38 eV; the oscillator strength is quite low and it is stabilized by 0.2 eV by applying the CASPT2 correction (7.18 eV). The three higher in energy electronic transitions involve the doubly occupied lower energy orbital, σ_1. Within this subset, the dynamic electronic correlation effects are among the largest observed for this system, in some cases reaching almost 1 eV. The σ_1-3s is an optically dark state at 7.94 eV (CASSCF), which is stabilized at 7.20 eV after CASPT2 correction. S_7, dominated by the σ_1-3p$_z$ configuration, has a CASSCF excitation energy of 8.47 eV, and a drop of about 1 eV is observed after perturbative correction. The highest-energy electronic transition at CASSCF level ($S_0 \rightarrow S_8$) is optically forbidden and appears at 8.84 eV; this transition still remains the highest-energy one upon CASPT2 correction (8.13 eV).
Thus, as shown in Table 2, the energetic order of the states found at CASSCF level of theory is not altered by inclusion of dynamic correlation, as one could expect for a set of Rydberg states not mixed to valence electronic transitions.

Ground state features: stored and activation energies

The minimum energy structures of NBD and QC in S_0 belong to the C_{2v} symmetry point group. The computed equilibrium geometries are in excellent agreement with experimental data, as attested by the good comparison between the determined structural parameters and the experimental ones in Table 4 in ESI and the harmonic vibrational frequencies analysis reported in ESI under Figure 6. At CASSCF level of theory, the Gibbs free energy difference between the QC and NBD isomers, corresponding to the stored energy upon the photoreaction (ΔE_{st}), is calculated to be 34.82 kcal/mol (1.51 eV), while the barrier for the thermal back reaction ($\Delta E^{\ddagger}$) is predicted at 29.06 kcal/mol (1.26 eV). A large contribution from dynamic electronic correlation is found for ΔE_{st}, that is 23.29 kcal/mol, being now in excellent agreement with the average of the experimental values (22 $\pm$1 kcal/mol).[37,38,58] On the contrary, the energy required for the back reaction is essentially unchanged upon perturbation, being 30.90 kcal/mol. The transition state (TS‡) connecting the reagent, NBD$_{minS_0}$, and the photoproduct, QC$_{minS_0}$, is located at 63.38 and 53.69 kcal/mol above the NBD energy, at CASSCF and CASPT2 levels, respectively, in good agreement with previous theoretical results (CCSD(T) energies on MP2/6-31G* optimized structures) reported in ref. 59 and no reaction intermediates are present, as expected. The transition state allowing the QC stored energy release is a diradical structure, where only one QC σ bond has been broken, and therefore belongs to the C_1 point group. The normal mode composition describing the imaginary Hessian eigenvalue (i1047.53 cm^{-1}) is shown in the inset of Figure 2 (blue arrows), highlighting the complex atom rearrangement. A quantitative comparison of the structural parameters is available in Table 4 in ESI.

Photochemical pathways: the effects of dynamic correlation

As above mentioned and shown in Table 1, the NBD absorption spectrum differs depending on the method applied, not only (as expected) in terms of energies, but also in terms of ordering of the electronic states. Especially, if a stabilization of the energy is expected, mostly for π,π* states, when including the dynamic electronic correlation through the CASPT2//CASSCF methodology, a modification of the states order affects not only the photophysics of the system (i.e., the absorption spectrum), but also and more importantly its photochemistry, that is, its chemical reactivity in the excited state. Indeed, CASPT2 (for both SS- and MS-formulations) stabilizes the dark V_1 state, that becomes the lowest-lying excited state (S_1), while at CASSCF level S_1 is a partially bright Rydberg state. Even, most importantly, the CASSCF sixth excited state, corresponding to the bright V_3, at MS-CASPT2 level lies just above the first Rydberg state (S_3), whereas the weakly bright V_2 double excitation is found much higher in energy (see Table 1). In terms of photochemistry, this means that the pathways calculated at CASSCF level might lead to a misleading description.[44] Indeed, we calculated the MS-CASPT2//CASSCF mimimum energy paths after vertical transition to the bright V_3 (Figure 3), to the weakly bright Rydberg π_2-3s and to the dark V_1 states (Figures 10 and 11 in ESI), which are the states of potential interest for solar energy absorption,

Table 2. QC absorption spectrum values: principal configuration for the first nine singlet states (S_n) and vertical excitation energies (eV) at CASSCF, SS- and MS-CASPT2 levels. The expectation values of second Cartesian moments ($\langle x^2\rangle$,$\langle y^2\rangle$,$\langle z^2\rangle$ in au^2) are given at CASSCF level. Oscillator strengths (f_{OSC}, dimensionless) are computed at CASSCF and MS-CASPT2 level.

E.S.	Configuration	CASSCF	f_{OSC}	$\langle x^2\rangle$	$\langle y^2\rangle$	$\langle z^2\rangle$	SS-CASPT2	MS-CASPT2	f_{OSC}
S_0	G.S. σ_1-σ_2	0.00	–	-27.04	-28.79	-28.85	0.00	0.00	–
S_1	RYD σ_2-3s,$3p_y$	5.70	$9.65*10^{-4}$	-36.98	-48.00	-39.47	5.75	5.70	$9.64*10^{-4}$
S_2	RYD σ_2-$3p_z$	6.31	–	-29.63	-31.85	-50.31	6.03	6.02	–
S_3	RYD σ_2-$3p_y$,$3d_{z^2}$	6.64	$5.32*10^{-3}$	-37.00	-48.25	-35.11	6.50	6.55	$5.24*10^{-3}$
S_4	RYD σ_2-$3p_x$,$3d_{xy}$	6.78	$4.74*10^{-4}$	-49.02	-39.35	-34.40	6.69	6.69	$4.68*10^{-4}$
S_5	RYD σ_2-$3d_{z^2}$,$3d_{x^2-y^2}$	7.38	$1.16*10^{-4}$	-38.67	-35.11	-40.39	7.18	7.18	$1.13*10^{-4}$
S_6	RYD σ_1-3s,$3p_y$	7.94	–	-39.63	-42.89	-41.59	7.19	7.20	–
S_7	RYD σ_1-$3p_z$	8.47	$2.46*10^{-3}$	-28.72	-33.02	-49.75	7.48	7.49	$2.17*10^{-3}$
S_8	RYD σ_1-$3p_x$,$3d_{z^2}$	8.84	–	-29.91	-55.77	-34.45	8.13	8.13	–

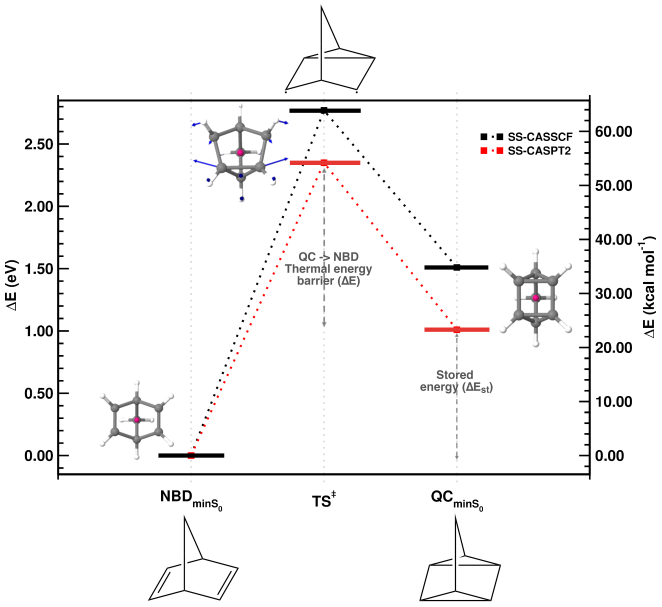

Figure 2. Relative energies in eV and kcal/mol of NBD$_{min\,S_0}$, TS‡ and QC$_{min\,S_0}$ structures optimized at CASSCF level (black) and corrected by CASPT2 (red). The normal mode composition which corresponds to the motion along the QC→NBD reaction coordinate, corresponding to thermal or catalyzed release of the stored energy, is shown by blue arrows. he Intrinsic Reaction Coordinate (IRC) is reported in Figure 7 in ESI.

although in the UV-region. All paths are shown as a function of the two coordinates described in the Computational details section, i.e., a distance and an angle between non-covalently bound carbon atoms. As evinced by all three paths, angle shrinking is always the initial driving coordinate, although different electronic states are involved in the isomerization, depending on the energy of the incoming photon. When populating by vertical transition the bright V_3 state, a small shrinking of the angle coordinate determines the formation of a three-state intersection, after which, following the minimum energy path, the doubly excited V_2 state can be populated due to the sloped topology of the crossing. Here we can observe a first difference compared to the CASSCF pathway, since at CASSCF level a three-state intersection is also found, but it involves V_1, V_2 and the Rydberg π_2-3s states, while at MS-CASPT2//CASSCF level V_1 is substituted by V_3, i.e., an optically dark state is substituted by a bright one. From the geometrical point of view, the population of V_2 sets the beginning of the coupling between angle shrinking and distance shortening, until ~~an avoided crossing (AC)~~ a crossing seam between V_2 and V_1 is reached (see Figure 5, left). Such ~~single-path crossing (an AC point is characterized by parallel derivative coupling and gradient difference vectors)~~ energy degeneracy leads to repulsion of V_2 and V_1 electronic characters and thus, V_2 population can be only transferred downhill to the V_1 state, ~~is reached from the upper electronic state (V_2) and due to the repulsion among the almost crossing states,~~ although several molecular vibrations are expected to take place at the V_2 minimum before populating the lower-in-energy V_1 state.[60] As is apparent in Figure 3, population of V_1 determines the termination of the angle-distance coupling, further decreasing the energy only along the distance coordinate, finally reaching a V_1/GS peaked CI, characterized by a tilt that should favor internal conversion back to NBD rather than the formation of QC (see Figure 5). Looking at the molecular rhomboidal distortion, this final S_1/S_0 CI corresponds to the Olivucci-Robb CI type previously described for photoactivated Diels-Alder reactions.[43] The characterization of the most relevant points along the NBD→QC photochemical path (section) can therefore rationalize the low quantum yield observed for the process, but also explain and guarantee the absence of byproducts.[8] As aforementioned, we have also calculated the minimum energy paths when irradiating the Rydberg π_2-3s state (Figure 10 in ESI), finding out that it follows exactly the same reactivity as when V_3 absorbs the photon, and when irradiating the lowest-energy excited state V_1 (Figure 11 in ESI), in this last case observing how it proceeds directly toward the mentioned V_2/V_1 crossing seam, this time rapidly crossing due to its TS-like structure.[60]

Although less interesting due to the lack of π electrons (and hence of the chemical concept of a π-conjugated chromophore), the photoinduced QC→NBD photo-reaction was also studied, since the description (usually neglected) of Rydberg states can explain such process, possibly being useful to envisage novel MOST systems based on the chemical substitution of the NBD/QC parent system. As discussed above, the CASSCF order of the excited electronic states is the same also for SS- and MS-CASPT2 methods, in any case leading to dark or almost dark vertical transitions. Hence, in principle, QC photo-reactivity can be safely described (at least qualitatively) by CASSCF, without the imperative need to include dynamic electronic correlation. Nevertheless, for a matter of comparison with the studied NBD→QC pathway, also in this case, the MS-CASPT2//CASSCF method was applied (Figure 4). The main novelty is the requirement of populating (moreover

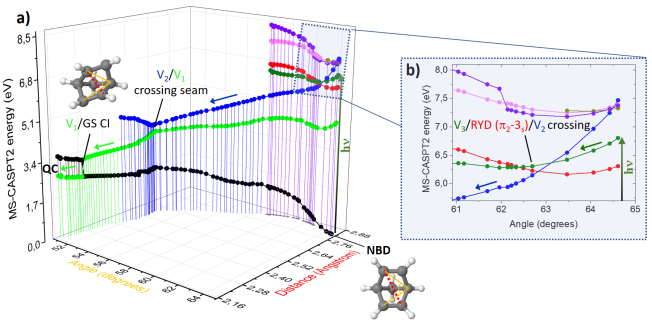

Figure 3. a) NBD→QC MS-CASPT2//CASSCF minimum energy path as a function of C-C "diagonal" distance (dotted red line) and C-C-C non-covalent angle (solid yellow line). The arrows describe the photo-reaction when irradiating the bright V_3 (π_1-π_3*) state, until the ground state is reached. b) Inset showing the first steps of the path leading to the first intersection region, as a function of the aforementioned angle. Color scheme: GS (π_1-π_2); RYD (π_2-3_s); V_1 (π_2-π_3*); V_2 (π_2-π_3*)$_2$; RYD (π_2-3_{dz^2}); RYD (π_1-3_{dz^2}); V_3 (π_1-π_3*); RYD (π_2-3_{py}); RYD (π_1-3_s).

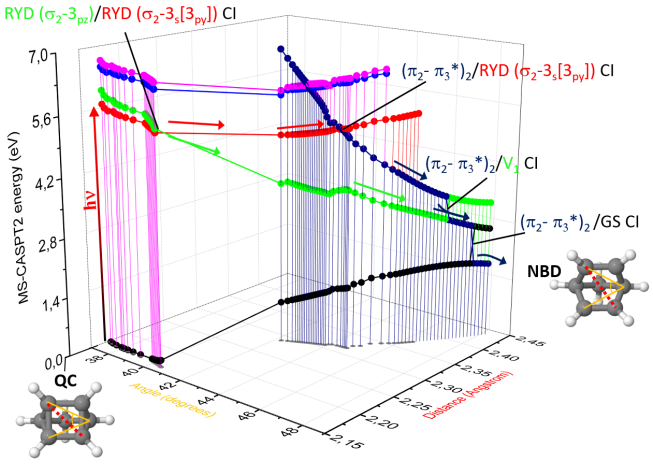

Figure 4. QC→NBD MS-CASPT2//CASSCF minimum energy path as a function of C-C "diagonal" distance (dotted red line) and C-C-C non-covalent angle (solid yellow line). The arrows describe the possible photo-reaction channels when irradiating the weakly bright RYD (σ_2-$3_s[3_{py}]$) state, until the ground state is reached. Color scheme: GS (σ_1-σ_2); RYD (σ_2-$3_s[3_{py}]$); RYD (σ_2-3_{pz}); RYD (σ_2-$3_{py}[3_{dz^2}]$); RYD (σ_2-$3_{px}[3_{dxy}]$). The electronic state reported in dark blue is mainly dominated by the (π_2-π_3*)$_2$ configuration, being the one responsible for NBD photoreversion.

through a small energy barrier on the RYD (σ_2-$3_s[3_{py}]$) state, slowing the process) a valence state of double π-π* character, being the only possibility to generate NBD. At the Franck-Condon region, this valence state is appearing only when including 12 roots in the SA-CASSCF calculations, corresponding to S_{11} and being available only for high-energy ultraviolet radiation, definitely out of the spectral range (14.12 eV by MS-CASPT2), thus explaining the QC suitability as MOST high energy isomer, capable of storing for long time part of the absorbed incoming photon.
More in detail, as it can be seen in Table 2, the only possible absorption below 7.0 eV involves the vertical transition to the RYD (σ_2-$3_s[3_{py}]$), corresponding to a bright transition of non-negligible intensity. A first relaxation, characterized by increasing of the angle coordinate, allows the mixing with the higher-energy RYD (σ_2-3_{pz}) state until a CI is reached, from where the initial population can split among the two crossing states, but in both cases leading to a further CI with the valence state of double π-π* character, finally funneling (through strong coupling of angle and distance coordinates) the population of the closed-shell configuration and thus formation of the low-energy isomer NBD.

NBD stationary points and PES crossings characterization

In this section we discuss the characterization of the minimum energy geometries and PES singularities, at the CASSCF level, observed along the MEP related to the NBD→QC photoreaction, considering the electronic states in the energy range within the bright valence state, V_3. Especially, we will focus our attention on the main structural variations with respect to the GS minimum, also analyzing the frontier molecular orbitals. All excited state geometries were optimized at CASSCF level (V_3 π_1-π_3*, RYD π_2-3s and V_2 (π_2-π_3*)$_2$). More in detail, the minimum energy structure on the V_2 excited state is located at 4.63 eV above the ground state minimum retaining the initial C_{2v} symmetry. The V_2 minimum structure is halfway between the NBD and QC ground state minima, i.e. the non-covalent C_4-C_6 distance is 0.34 Å shorter than NBD (2.47 Å), the CC double bond length is 1.50 Å towards QC (C-C, 1.54 Å) while the four C-H bonds in the molecular plane undergo a remarkable pyramidalization ($\gamma_{min\,V_2}$: 26°; $\gamma_{min\,G.S.}$: 3.5°). Due to the shortening of the two pairs of distal carbons, favorable interactions between the p orbitals are evident going from the HOMO to the LUMO (see Figure 8 in ESI) and, as stated by Antol[43], these features confer to the stationary point a homosymmetric biradicaloid character. The minimum energy geometry for the lowest-energy Rydberg state, is computed at 5.99 eV, being stabilized by 0.58 eV with respect to the vertical transition energy (see Figure 8 in ESI). The structure still belongs to the C_{2v} symmetry and exhibits some few differences when compared to the previous case. The molecular plane identified by the $C_{4(5)}$-$C_{7(6)}$ carbon atoms distances is 0.09 Å larger than the V_2 minimum structure and the CC double bond length is 1.38 Å, much similar to the value computed for the ground state minimum (1.35 Å). The four hydrogen atoms at the top of the molecular plane undergo only a slight pyramidalization, $\gamma_{min\,Ryd}$: 10°. On the contrary, to reach the minimum energy structure of the bright valence state (V_3, at 8.04 eV) an opposite trend is observed, i.e. the carbon atoms that identify the molecular plane, $C_{4(5)}$-$C_{6(7)}$, are located at a greater distance (0.02 Å) with respect to the ground state minimum, 2.82 Å and the four related -CH bonds are now turned more towards the -CH_2 bridge ($\gamma_{min\,V_3}$: ∼-7.00°). Accordingly, the p orbitals forming π_3 are more localized and less interacting, see Figure 8 in ESI. Considering the evolution of the reaction coordinates mainly involved during photorelaxation, it is plausible that the V_3 minimum geometry is sparsely populated. A summary of main structural changes between stationary points discussed above is reported in Table 5 in ESI.
Additionally, from a careful analysis of the wavefunction composition for the π_2-3s equilibrium geometry, it is important to underline that at CASSCF level we are witnessing the degeneration of three excited states namely the Rydberg π_2-3s state and two valence states V_1 (π_2-π_3*) and

V_2 $(\pi_2\text{-}\pi_3^*)_2$ around 6.00 eV, suggesting the presence of a PES singularity. To search for this crossing region we used the PCO approach by imposing an energetic constraint between the first three excited states. Once convergence is reached, from the CASSCF wavefunction analysis, the energy gap between the V_1 (π_2-π_3^*), Rydberg π_2-3s and V_2 $(\pi_2\text{-}\pi_3^*)_2$ states, placed at 5.99 eV, is actually zero. Further confirmations are obtained by considering the value of the norm of the non adiabatic coupling matrix elements which is very high between the V_2 and V_1 states. The V_2/V_1 crossing ~~is an avoided crossing~~ constitutes a seam as it is shown in Figure 5~~, left~~. ~~the two non-adiabatic vectors form in general an angle between them, determining the characteristic branching plane that allows the formation of one (or more) photoproducts. Nevertheless, it is also possible that the two vectors are parallel (i.e., forming an angle of 0 or 180 degrees), and in this case no branching plane can be determined, thus generating repulsion between the crossing electronic states.~~ This opens up two possible scenarios: (i) if approaching the ~~AC~~ crossing seam from the upper-energy state (in this case from V_2), some vibrations in the ~~AC~~ V_2 minimum region are necessary before population of the lower-energy state; (ii) if approaching the ~~AC~~ seam from the lower-energy state (in this case from V_1), a transition state-like structure replaces the crossing (that is ~~indeed~~formally avoided) if the topology corresponds to nonadiabatic tunneling type crossing or, as it is the case here, the almost-zero coupling between the crossing states corresponds to a Landau-Zener type crossing, i.e. the system continues relaxing on V_1 without energy minima[61]. Indeed, when optimizing the V_1 state, no energy minima are found, leading from the Franck-Condon region directly to a CI with the ground state (Figure 5, left, at 4.21 eV, at CASSCF level) which acts as a relaxation funnel, coherently with the CASPT2 picture. In this case, two opposite carbon atoms are mainly involved, namely C_4 and C_6, which converge to a rhombohedral geometry for which, the two C-H bonds on the minor diagonal exhibit a fair pyramidalization. Furthermore, the HOMO and LUMO frontier orbitals change drastically with respect to the previous cases becoming localized on each corner of the plane and non interacting. The structural parameters, the CI geometry and frontier molecular orbitals are reported in Table 4 and Figure 8 in ESI, respectively.

However, as shown in Figures 3 and 7 the inclusion of the dynamic correlation through the second order perturbation theory leads to a greater stabilization of the valence states involved, thus significantly modifying the CASSCF picture. Nevertheless, it is worth noting that all involved geometries show that the most important set of internal coordinates that guide the relaxation to the excited state minima or towards the crossing regions are mainly the shortening of the carbon atoms in the molecular plane (through both distance and angle between non-covalent atoms) and the simultaneous pyramidalization of the four hydrogen atoms to which they are bound.

According to the systematic characterization of PES singularities of Galván and coworkers[62] the V_2/V_1 ~~AC~~ crossing seam and the V_1/GS CI found downhill after vertical excitation show that, although the ~~AC~~ crossing seam should slightly slow down the velocity of the process, its Landau-Zener topology description (i.e., the energy gradient sign of V_1 does not change when passing through the ~~AC~~ crossing seam) ensures evolution of the system toward the CI with the electronic closed-shell GS configuration. This CI has a peaked topology, tilting mainly toward the recovering of NBD (i.e., conferring photostability to the system by non-radiative internal conversion), but also opening a less probable but available channel leading to QC formation, confirming the non-negligible NBD→QD photoproduction quantum yield, found experimentally.[63] For a full description of the topographical parameters of each crossing reported in Table 6 in ESI, please refer to Ref. 62. For a graphical explanation of ~~the difference between CI and AC~~ the different type of crossing and their possible population evolution, please refer to Ref. 60 (Scheme 2).

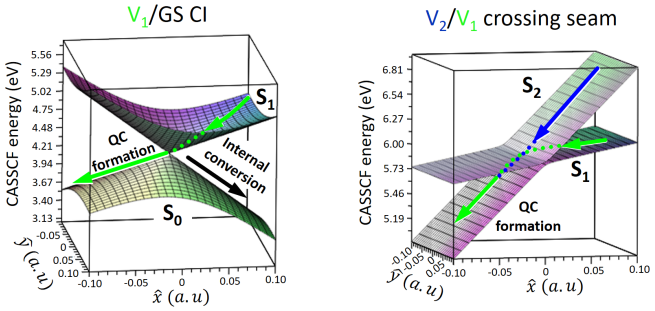

Figure 5. Graphical representation of the electronic surfaces around the V_2/V_1 ~~AC~~ crossing seam (right) and the V_1/GS CI (left), experienced by both CASSCF and CASPT2 descriptions, with the CASSCF energy as a function of two vectors, $\hat{x}$ and $\hat{y}$, corresponding to vectors spanning the branching plane defined by the non-adiabatic coupling vectors, i.e., derivative coupling and gradient difference vectors. The colored arrows pictorially sketch the possible non-adiabatic photoreactive paths, following the same color code as in Figure 3.

Potential energy surfaces along representative reaction coordinates

In this section we address and discuss the MS-CASPT2//CASSCF potential energy photodeactivation pathways of NBD and QC, only considering the two relevant and strongly coupled reaction coordinates, namely, the shortening and lengthening of two non-covalent carbon atoms placed in the six-carbons ring and the opening and closing of the non-bonding C-C-C angles.

This step is fundamental if one wishes to decrease the dimensionality problem of the NBD-QC system to only two dimensions. This is important not only for an easier description of an inherently complex reactivity, but also as preparatory step to further build simplified but reliable potential energy surfaces, on top of which analytical semi-classical photo-dynamics would make possible to study the system also from the kinetic point of view, apart from the thermodynamic one, shown in this work.

For this purpose, relaxed scans were performed along selected non-dark excited states, as better explained in the Computational details section, all the graphs report only the non-bonding C-C-C angles for a better reading. The relaxed scans computed at CASSCF level are reported in Supporting Information (see Figure 12 to Figure 15). Numerous attempts have been made trying to decouple the two reaction coordinates by initially proceeding from the shrinking of the C-C-C angle and then considering only the non-bonding distance C-C that leads to the formation of the CI between the GS and V_1 states. The results obtained from

preliminary tests highlighted that the photo-relaxation from any non-dark excited states is not physically sound as suspicious inversions of the GS and V_1 curves close to the FC geometry were observed. The valence and Rydberg excited states computed at MS-CASPT2 level when the photorelaxation occurs on the low-lying Rydberg excited state is shown in Figure 6. Taking into account both the reaction coordinates, some features observed in the related MEP (see Figure 10 in ESI) are reliably described. In depth, we refer for example to the first degeneration zone that involves the bright valence state V_3 and the $(\pi_2\text{-}\pi_3^*)_2$ doubly excited state at $\sim$ 6.50 eV nearby the FC point and to the subsequent CI at lower energy ($\sim$ 5.95 eV) between the V_2 and the first Rydberg excited state. On the contrary, the funnel between the V_2 and V_1 valence states, computed below 5.00 eV in the MEP in Figure 10 in ESI is not present. Finally, upon geometric deformations that mainly involve the C_4-C_6 non-bonding distance, a degeneration is observed between the ground state and the first dark valence state at 2.120 Å and 51°. A significantly different scenario is present at CASSCF level, see Figure 12 in ESI, highlighting also in this case the crucial role played by dynamic electronic correlation effects on photophysics.

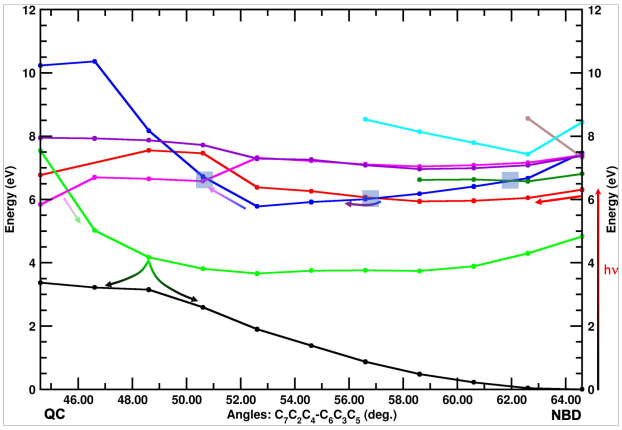

Figure 6. NBD→QC MS-CASPT2//CASSCF diabatic potential energy curves scanning simultaneously the $C_7C_2C_4$-$C_6C_3C_5$ non-bonding angle and the C_4-C_6 non-bonding distance along the (π_2-3_s) Rydberg excited state. Color scheme: GS (π_1-π_2); RYD (π_2-3_s); V_1 (π_2-π_3); V_2 (π_2-π_3^*)$_2$; RYD (π_2-3_{dz^2}); RYD (π_1-3_{dz^2}); V_3 (π_1-π_3); RYD (π_2-3_{py}); RYD (π_1-3_s).

The MS-CASPT2 relaxed scan upon the excitation on the V_3 (π_1-π_3) bright valence state taking into account both the reaction coordinates variations is reported in Figure 7. For the reference one at CASSCF level we refer to Figure 13 in Supporting Information. The photorelaxation from the FC region initially takes place on the V_3 state, which degenerates almost immediately with the first Rydberg and the doubly excited states leading to an overlap zone just above 6 eV, as seen in Figure 3 panel B. In this region we are witnessing the population of the doubly excited state, V_2, which undergoes a discrete stabilization in energy approaching to the underlying dark valence state around 55° as similarly captured by the related MEP discussed above. Concerning the remaining excited states, the PESs profiles show no significant variation, but remain roughly smooth in the interval considered. Proceeding further towards the formation of the QC photoproduct we observe the key role of the V_2 state in populating the valence state which is dark upon UV irradiation. Unlike the MEP discussed above, in the region below 45° the PESs obtained by considering the two reaction coordinates coupled during the relaxation show the superposition of the strongly destabilized ground state with the first valence state and the doubly excited valence around 4 eV. For both the overlap regions however, the NBD distorts becoming almost structurally similar to the CI geometries reported in Figure 8 in ESI.

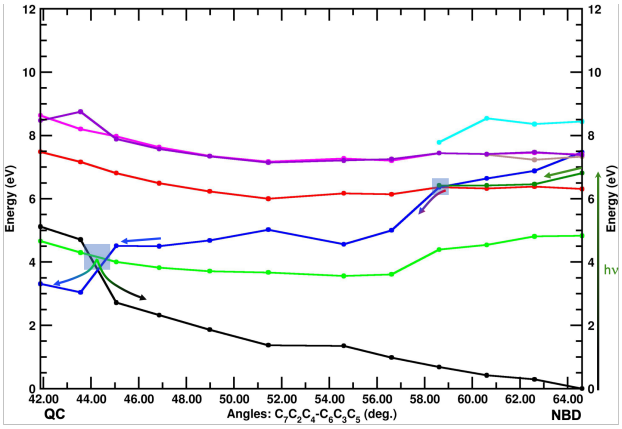

Figure 7. NBD→QC MS-CASPT2//CASSCF diabatic potential energy curves scanning simultaneously the $C_7C_2C_4$-$C_6C_3C_5$ non-bonding angle and the C_4-C_6 non-bonding distance along the V_3 (π_1-π_3) bright valence state. Color scheme: GS (π_1-π_2); RYD (π_2-3_s); V_1 (π_2-π_3); V_2 (π_2-$\pi_3{}^*)_2$; RYD (π_2-3_{dz^2}); RYD (π_1-3_{dz^2}); V_3 (π_1-π_3); RYD (π_2-3_{py}); RYD (π_1-3_s).

The possible reverse QC→NBD photoinduced isomerization was also studied in terms of relaxed scans along the two reaction coordinates described above. In Figure 14 in ESI we report the potential energy curves computed at CASSCF level on the ground state along the solely $C_7C_2C_4$-$C_6C_3C_5$ reaction coordinate in QC (the analogous relaxed scan performed stretching the C_4-C_6 distance did not converge). A greater accuracy is achieved, at a reasonable computational cost, when the second order perturbative correction is applied on top of the CASSCF wavefunction. The excited states energies computed along the ground state relaxed scan are reported in Figure 8. A smooth S_0 profile allows to reach the region of the transition state, where the electronic nature of S_0 changes from the closed-shell GS to a (π_2-$\pi_3{}^*)_2$ electronic state that allows QC→NBD energy release by forming back the two π bonds of NBD. The energy barrier is calculated at 1.49 eV, hence only slightly overestimating the value obtained by full optimization of TS and QC (ca. 1.35 Å, see Figure 2).

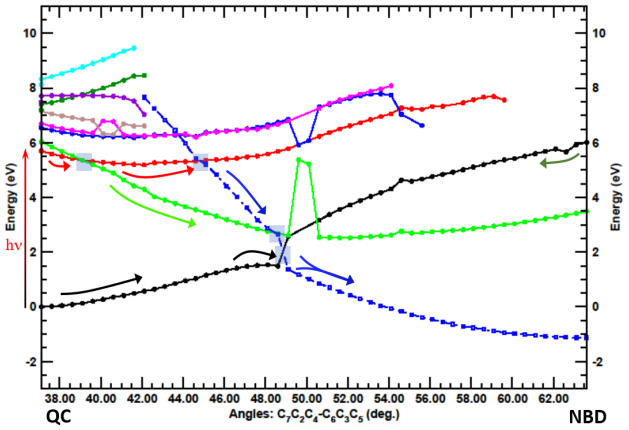

Figure 8. QC→NBD MS-CASPT2//CASSCF diabatic potential energy curves scanning the $C_7C_2C_4$-$C_6C_3C_5$ non-bonding angle along the GS. Color scheme: GS (σ_1-σ_2); RYD (σ_2-$3_s[3_{py}]$); RYD (σ_2-3_{pz}); RYD (σ_2-$3_{py}[3_{dz^2}]$); RYD (σ_2-$3_{px}[3_{dxy}]$); RYD (σ_2-$3_{dz^2}[3_{dx^2-y^2}]$); RYD (σ_1-$3_s[3_{py}]$); RYD (σ_1-3_{pz}); RYD (σ_1-$3_{px}[3_{dz^2}]$). The electronic state reported in blue with dashed line and squares is mainly dominated by the (π_2-$\pi_3{}^*)_2$ configuration.

The RYD (σ_2-$3_s[3_{py}]$) state constitutes the most probable way to revert photochemically the QC isomerization, both the two relevant coordinates discussed above were scanned on this Rydberg state. The CASSCF related scan is reported in under Figure 15 in ESI. Upon CASPT2 correction (see Figure 9), we find that such Rydberg state acts as a population channel for the underlying electronic states that are very close in energy in the FC point. The electronic states around 8 eV undergo a sudden increase in energy, while the two Rydberg states ((σ_2-$3_{px}[3_{dxy}]$) and σ_2-$3_{dz^2}[3_{dx^2-y^2}]$)) tend to be degenerate in the range explored. Several paths can be potentially undertaken: by overcoming a negligible energy barrier, it is possible to populate the doubly excited state which begins to be present for small geometric distortions; alternatively, following an efficient population of the (σ_2-3_{pz}) and (σ_2-$3_{py}[3_{dz^2}]$) states it is possible to reach the ground state PES and then proceed thermally to the formation of the NBD progenitor. To summarize, when looking at the QC→NBD photoprocess, we note that the key to accomplish isomer photoreversion is the population of the (π_2-$\pi_3{}^*)_2$ state, placed high in energy in the QC minimum region (higher than S_8), but decreasing in energy with a high slope as a function of the scanned angle, until forming a conical intersection with the GS. There are in principle two possible paths to populate the (π_2-$\pi_3{}^*)_2$ state within the limits of the solar UV spectral range: (i) most likely, by vertical transition to the weakly bright Rydberg state (σ_2-$3_s[3_{py}]$), that crosses almost immediately (below 40°) with the dark RYD (σ_2-3_{pz}) state at ∼5.60 eV, and then reaches an excited state minimum, with a really small barrier (below 0.1 eV) to populate the double excited state; (ii) less likely, by vertical transition to the dark RYD (σ_2-3_{pz}), that proceeds downward in energy until intersecting the double excited state in the nearby of its minimum.

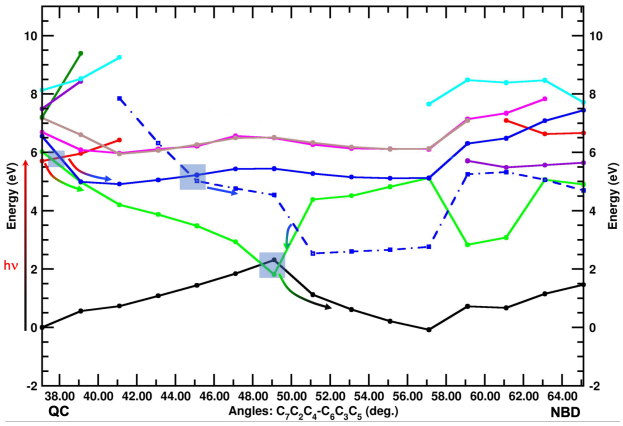

Figure 9. QC→NBD MS-CASPT2//CASSCF diabatic potential energy curves scanning simultaneously the $C_7C_2C_4$-$C_6C_3C_5$ non-bonding angle and the C_4-C_6 non-bonding distance along the (σ_2-$3_s[3_{py}]$) Rydberg excited state. Color scheme: GS (σ_1-σ_2); RYD (σ_2-$3_s[3_{py}]$); RYD (σ_2-3_{pz}); RYD (σ_2-$3_{py}[3_{dz^2}]$); RYD (σ_2-$3_{px}[3_{dxy}]$); RYD (σ_2-$3_{dz^2}[3_{dx^2-y^2}]$); RYD (σ_1-$3_s[3_{py}]$); RYD (σ_1-3_{pz}); RYD (σ_1-$3_{px}[3_{dz^2}]$). The electronic state reported in blue with dashed line and squares is mainly dominated by the (π_2-π_3^*)$_2$ configuration.

Conclusion

In the present work, we studied the ground and excited state chemistry determining the norbonadiene⇔quadricyclane isomerization cycle, which constitutes, until now, the most relevant building block to design molecular solar-thermal (MOST) systems. In order to address such issues, we relied on the multiconfigurational complete active space self-consistent field (CASSCF) calculations, including dynamic correlation effects by means of second order perturbation theory (CASPT2). We found that the inclusion of dynamic electron correlation is mandatory to avoid a misleading description of the photochemical pathways as it affects the energetic order of the excited states and, as a consequence, the overall description of the relaxation channels. Remarkably we also demonstrated that the accurate description of photochemical phenomena requires taking into account the low-energy Rydberg states, most of the times excluded in previous studies. Especially, we accurately modelled the valence and 3s, 3p, 3d Rydberg excited states of NBD and QC by adding contracted diffused basis functions in the center of gravity of the charges of both reagent and photoproduct. The ground state (thermal) pathway was studied with the same level of theory, predicting thermal energy barrier and stored energy to be in excellent agreement with the experimental data and also with higher level theoretical calculations.

Concerning NBD→QC photorelaxation, two coupled reaction coordinates are mainly relevant to describe all phenomena. The role played by Rydberg-type excited states proved to be crucial since, after irradiation, they act as non-adiabatic population channels for the valence excited states mainly involved in the formation of the new chemical bonds of the quadricyclane photoproduct. We also found that, the light-induced back isomerization reaction (from QC to NBD) mainly involves low energy Rydberg states and, as observed for the thermal pathway, a doubly excited valence state governs and mediates the final population of the ground state. Also, we simplified the dimensionality of such complex system computing relaxed potential energy surface scans along the two aforementioned coupled coordinates, describing the symmetric closure/opening of the angle between non-covalent carbons and the shrinking/lengthening of the "diagonal" non-covalent carbon-carbon distance, respectively. We could identify the former as the initial driving NBD→QC coordinate leading the photorelaxation from the Franck-Condon region to the first intersection region, followed by a high coupling of the two coordinates leading to the final conical intersection with the ground state, where the latter becomes ultimately the dominant coordinate. Also the reverse NBD→QC eventual photochemistry can be satisfactorily described by the above mentioned coordinates. This opens the way toward the computationally efficient and quantitatively reliable photodynamical study of the NBD/QC system, and eventually of its main derivatives, proposed as potential solar-thermal fuels.

Computational details

The ground state equilibrium structures of NBD and QC optimized in gas phase at CASSCF(4,4)/6-31G(d) level of theory, have been retrieved from a recently published paper by some of the authors [36] and employed as starting point for the present work. The ANO-L basis set contracted to C[3s2p1d]/H[2s1p] was employed and, to get a more accurate description of the low-lying Rydberg states, it was augmented by one set of [1s1p1d] diffuse orbitals (reported in Table 3 in ESI) contracted from a set of 8s8p8d primitives, with Kaufmann coefficients [64] centered on a fictitious atom placed in the center of charge of each molecule [65,66]. The contraction scheme considered here allowed to restrict the Rydberg orbitals to a single set of $3s$, $3p$ and $3d$ orbitals, thus reducing the computational cost and facilitating the assignment of electronic transitions.

The zero-order electronic wavefunction has been calculated by State-Average Complete Active Space Self Consistent Field (SA-CASSCF) calculations, averaging over the first nine singlet roots. After preliminary tests on the composition of the active space and number of excited states to include in the average (see Figure 1 in ESI), a CASSCF(4,7), i.e. 4 electrons and 7 orbitals, was used for both NBD and QC systems (Figure 2 to Figure 5 in ESI), representing a good compromise between the computational burden and the quality of the zero-order wavefunction.

Dynamic electronic correlation effects were accounted for by single-state (SS-) and multistate (MS-) CASPT2 calculations, keeping frozen, at perturbative level, the $1s$ orbitals of the carbon atoms.

The MS-CASPT2 vertical excitation energy and oscillator strength were also computed at NBD geometry with the default IPEA shift (0.25 E_h) applied to the zeroth-order Hamiltonian, see Table 2 in ESI for comparison. In what follows, the CASPT2 calculations are to be considered without IPEA shift. The computed nine roots (i.e., the ground state S_0 and the lowest-lying 8 singlet excite states, S_1-S_8) were included in the MS-CASPT2 calculations and a real shift of 0.25 au has been used to remove eventual intruder states and thus potential energy surface discontinuities. [67] The CASSCF state interaction method has been used to compute transition dipole moments (TDM) and oscillator strengths (f_{OSC}), and the corresponding quantities at MS-CASPT2 level have been obtained according to the equation: f=2/3(TDM$_{CASSCF}$)$^2\Delta E_{CASPT2}$, where ΔE_{CASPT2}

corresponds to the CASPT2 energy difference between the ground state and the excited state of interest.

Relevant excited state stationary points, minimum energy conical intersections (CI) and crossing seam, optimized within the projected constrained optimization (PCO) method, have been also obtained and characterized at CASSCF(4,7)//ANO-L+1s1p1d level, while their energy was corrected *a posteriori* through single point CASPT2 calculations. Also on the electronic ground state, the two minima (NBD and QC) and the first order saddle point (i.e., the transition state) have been optimized following the same CASPT2//CASSCF strategy. For the saddle point search, the two C_4-C_7 and C_5-C_6 distances have been initially constrained at 1.750 and 2.400 Å, respectively (the numbering scheme is reported in Figure 1) and then relaxed freely.

CASPT2//CASSCF minimum energy paths (MEPs) for all excited states (S_1-S_8) were finally calculated to investigate both NBD⇒QC and QC⇒NBD pathways (results shown only for the reactive pathways).

The MEPs analysis allowed us to identify two main reaction coordinates, the C_4-C_6 distance and two angles symmetrically arranged between non-covalent carbon atoms ($C_7C_2C_4$ and $C_6C_3C_5$), along which CASPT2//CASSCF relaxed potential energy scans have been performed for all the considered states. A scan step of ±0.07 Å for the distance and of ±2.0° for both angles was simultaneously used (minus sign refers to NBD reactivity) to take into account the coupling of the two reaction coordinates involved in the photorelaxation. In particular, upon NBD excitation, the potential energy curves along the C_4-C_6 distance have been calculated from 2.78 to 1.82 Å, while along the $C_7C_2C_4$ and $C_6C_3C_5$ symmetric angles, the scans ranged from 64.1 to 37.1°; vice versa upon QC photoexcitation.

At each CASSCF optimized crossing point, non-adiabatic coupling vectors (i.e., derivative coupling and gradient difference vectors) between the intersecting states have been computed, and, for the most relevant cases, the topology around the CI was depicted. The weight of the CASSCF reference wavefunction in the CASPT2 results has been regularly checked for all electronic states along each scanned coordinate and each minimum energy path, to exclude the presence of intruder states, and it was always satisfactorily found to be between 76 and 78%. Along the relaxed scans few *ad-hoc* constraints (reported in Figure 9 in ESI) have been imposed to prevent displacements of the dummy atom to which the diffuse basis was assigned.

All the calculations have been performed by using the OpenMolcas electronic structure software package.[68,69] Considering a previous robust study on the same molecular system by Jorner et al.,[41] the CASSCF method can correctly describe the main characteristics of the NBD/QC system. Hence, although while performing the present study analytical CASPT2 gradients were made available for OpenMolcas,[70] we can firmly state that our CASPT2//CASSCF approach is highly reliable, also considering our extended active space and higher number and type of electronic excited states.

Acknowledgements

F.C., D.R. and M.P. acknowledge financial support through the COMETE project (COnception in silico de Matériaux pour l'EnvironnemenT et l'Energie) co-funded by the European Union under the program FDER-FSE Lorraine et Massif des Vosges 2014-2020. M.N. is grateful to the Spanish Ministry of Science, Innovation and Universities for a doctoral fellowship. M.M. thanks the Comunidad the Madrid and the Universidad de Alcalá for funding through the project CM/JIN/2021-022 "SolFuel".

Conflict of Interest

There are no conflicts of interest to declare.

Keywords: ab-initio photochemistry • solar energy storage • MOST • CASSCF • CAS-PT2

References

[1] N. Armaroli, V. Balzani, Chem. Eur. J. **2016**, 22, 32.
[2] Y. Tachibana, L. Vayssieres, J. R. Durrant, Nat. Photonics **2012**, 6, 511.
[3] K. Moth-Poulsen, D. Ćoso, K. Börjesson, N. Vinokurov, S. K. Meier, A. Majumdar, K. P. C. Vollhardt, R. A. Segalman, Energ. Environ. Sci. **2012**, 5, 8534.
[4] D. Zhitomirsky, E. Cho, J. C. Grossman, Adv. Energy Mater. **2016**, 6, 1502006.
[5] T. J. Kucharski, N. Ferralis, A. M. Kolpak, J. O. Zheng, D. G. Nocera, J. C. Grossman, Nat. Chem. **2014**, 6, 441.
[6] Z.-i. Yoshida, J. Photochem. **1985**, 29, 27.
[7] V. A. Bren', A. D. Dubonosov, V. I. Minkin, V. A. Chernoivanov, Russ. Chem. Rev. **1991**, 60, 451.
[8] A. D. Dubonosov, V. A. Bren, V. A. Chernoivanov, Russ. Chem. Rev. **2002**, 71, 917.
[9] A. Lennartson, A. Roffey, K. Moth-Poulsen, Tetrahedron Lett. **2015**, 56, 1457.
[10] Z. Wang, A. Roffey, R. Losantos, A. Lennartson, M. Jevric, A. U. Petersen, M. Quant, A. Dreos, X. Wen, D. Sampedro, et al., Energ. Environ. Sci. **2019**, 12, 187.
[11] A. E. Telgerafchi, M. Mehranpour, H. Nazockdast, Polym. Eng. Sci. **2021**.
[12] A. U. Petersen, A. I. Hofmann, M. Fillols, M. Mansø, M. Jevric, Z. Wang, C. J. Sumby, C. Müller, K. Moth-Poulsen, Adv. Sci. **2019**, 6, 1900367.
[13] S. Wu, H.-J. Butt, Macromol. Rapid Commun. **2020**, 40, 1900413.
[14] V. Caia, G. Cum, R. Gallo, V. Mancini, E. Pitoni, Tetrahedron Lett. **1983**, 24, 3903.
[15] C.-L. Sun, C. Wang, R. Boulatov, ChemPhotoChem **2019**, 3, 268.
[16] G. Jones II, T. E. Reinhardt, W. R. Bergmark, Sol. Energy **1978**, 20, 241.
[17] G. Ganguly, M. Sultana, A. Paul, J. Phys. Chem. Lett. **2018**, 9, 328.
[18] A. M. Kolpak, J. C. Grossman, J. Chem. Phys. **2013**, 138, 034303.
[19] Z. Wang, R. Losantos, D. Sampedro, M.-a. Morikawa, K. Börjesson, N. Kimizuka, K. Moth-Poulsen, J. Mater. Chem. A **2019**, 7, 15042.
[20] L. Dong, Y. Feng, L. Wang, W. Feng, Chem. Soc. Rev. **2018**, 47, 7339.
[21] M. B. Nielsen, N. Ree, K. V. Mikkelsen, M. Cacciarini, Russ. Chem. Rev. **2020**, 89, 573.
[22] O. Brummel, F. Waidhas, U. Bauer, Y. Wu, S. Bochmann, H.-P. Steinrück, C. Papp, J. Bachmann, J. Libuda, J. Phys. Chem. Lett. **2017**, 8, 2819.
[23] M. Jevric, Z. Wang, A. U. Petersen, M. Mansø, C. J. Sumby, M. B. Nielsen, K. Moth-Poulsen, Eur. J. Org. Chem. **2019**, 2019, 2354.
[24] M. J. Kuisma, A. M. Lundin, K. Moth-Poulsen, P. Hyldgaard, P. Erhart, J. Phys. Chem. C **2016**, 120, 3635.
[25] M. Mansø, A. U. Petersen, Z. Wang, P. Erhart, M. B. Nielsen, K. Moth-Poulsen, Nat. Commun. **2018**, 9, 1.
[26] M. Jevric, A. U. Petersen, M. Mansø, S. Kumar Singh, Z. Wang, A. Dreos, C. Sumby, M. B. Nielsen, K. Börjesson, P. Erhart, et al., Chem.-Eur. J **2018**, 24, 12767.
[27] U. Jacovella, E. Carrascosa, J. T. Buntine, N. Ree, K. V. Mikkelsen, M. Jevric, K. Moth-Poulsen, E. J. Bieske, J. Phys. Chem. Lett. **2020**, 11, 6045.
[28] O. Brummel, D. Besold, T. Döpper, Y. Wu, S. Bochmann, F. Lazzari, F. Waidhas, U. Bauer, P. Bachmann, C. Papp, et al., ChemSusChem **2016**, 9, 1424.
[29] U. Bauer, S. Mohr, T. Döpper, P. Bachmann, F. Späth, F. Düll, M. Schwarz, O. Brummel, L. Fromm, U. Pinkert, et al., Chem. Eur. J. **2017**, 23, 1613.
[30] V. Gray, A. Lennartson, P. Ratanalert, K. Börjesson, K. Moth-Poulsen, Chem. Commun. **2014**, 50, 5330.
[31] Y. Kanai, V. Srinivasan, S. K. Meier, K. P. C. Vollhardt, J. C. Grossman, Angew. Chem. Int. Ed. **2010**, 49, 8926.
[32] K. Börjesson, A. Lennartson, K. Moth-Poulsen, J. Fluor. Chem. **2014**, 161, 24.
[33] A. Lennartson, A. Lundin, K. Börjesson, V. Gray, K. Moth-Poulsen, Dalton Trans. **2016**, 45, 8740.
[34] R. D. Bach, I. L. Schilke, H. B. Schlegel, J. Org. Chem. **1996**, 61, 4845.
[35] C. Qin, Z. Zhao, S. R. Davis, J. Mol. Struct. THEOCHEM **2005**, 728, 67.
[36] M. Nucci, M. Marazzi, L. M. Frutos, ACS Sustain. Chem. Eng. **2019**, 7, 19496.
[37] D. S. Kabakoff, J. C. Buenzli, J. F. Oth, W. B. Hammond, J. A. Berson, J. Am. Chem. Soc. **1975**, 97, 1510.
[38] W. Steele, J. Chem. Thermodyn. **1978**, 10, 919.
[39] R. Kan, Organic photochemistry, McGraw-Hill **1966**.
[40] M. Schwarz, C. Schuschke, T. N. Silva, S. Mohr, F. Waidhas, O. Brummel, J. Libuda, Rev. Sci. Instrum. **2019**, 90, 024105.
[41] K. Jorner, A. Dreos, R. Emanuelsson, O. El Bakouri, I. F. Galván, K. Börjesson, F. Feixas, R. Lindh, B. Zietz, K. Moth-Poulsen, et al., J. Mater. Chem. A **2017**, 5, 12369.
[42] W. Fuß, K. K. Pushpa, W. E. Schmid, S. A. Trushin, Photochem. Photobiol. Sci. **2002**, 1, 60.
[43] I. Antol, J. Comput. Chem. **2013**, 34, 1439.
[44] A. Valentini, S. van den Wildenberg, F. Remacle, Phys. Chem. Chem. Phys. **2020**, 22, 22302.
[45] V. A. Petrov, N. V. Vasil'ev, Curr. Org. Synth. **2006**, 3, 215.
[46] F. Rudakov, P. M. Weber, J. Chem. Phys. **2012**, 136,

134303.
[47] B. O. Roos, M. Merchan, R. McDiarmid, X. Xing, J. Am. Chem. Soc. **1994**, 116, 5927.
[48] X. Xing, A. Gedanken, A.-H. Sheybani, R. McDiarmid, J. Phys. Chem. **1994**, 98, 8302.
[49] R. P. Frueholz, W. M. Flicker, O. A. Mosher, A. Kuppermann, J. Chem. Phys. **2008**, 70, 1986.
[50] B. Helmich-Paris, J. Chem. Theory Comput. **2019**, 15, 4170.
[51] M. Schreiber, M. R. Silva-Junior, S. P. Sauer, W. Thiel, J. Chem. Phys. **2008**, 128, 134110.
[52] I. Schapiro, K. Sivalingam, F. Neese, J. Chem. Theory Comput. **2013**, 9, 3567.
[53] M. R. Silva-Junior, M. Schreiber, S. P. Sauer, W. Thiel, J. Chem. Phys. **2010**, 133, 174318.
[54] M. R. Silva-Junior, S. P. Sauer, M. Schreiber, W. Thiel, Mol. Phys. **2010**, 108, 453.
[55] R. Sarkar, P.-F. Loos, M. Boggio-Pasqua, D. Jacquemin, Journal of Chemical Theory and Computation **2022**, 18, 2418.
[56] H.-D. Martin, C. Heller, E. Haselbach, Z. Lanyjova, Helv. Chim. Acta **1974**, 57, 465.
[57] E. Haselbach, H.-D. Martin, Helv. Chim. Acta **1974**, 57, 472.
[58] K. Raghavachari, R. C. Haddon, H. D. Roth, J. Am. Chem. Soc. **1983**, 105, 3110.
[59] R. D. Bach, I. L. Schilke, H. B. Schlegel, J. Org. Chem. **1996**, 61, 4845.
[60] M. Marazzi, U. Sancho, O. Castano, L. M. Frutos, Phys. Chem. Chem. Phys. **2011**, 13, 7805.
[61] H. Nakamura, Soryushiron Kenkyu Electronics **1990**, 80, E71.
[62] I. Fdez. Galván, M. G. Delcey, T. B. Pedersen, F. Aquilante, R. Lindh, J. Chem. Theory Comput. **2016**, 12, 3636.
[63] C. A. Farfan, D. B. Turner, Phys. Chem. Chem. Phys. **2020**, 22, 20265.
[64] K. Kaufmann, W. Baumeister, M. Jungen, J. Phys. B: At. Mol. Opt. Phys. **1989**, 22, 2223.
[65] B. O. Roos, K. Andersson, M. P. Fulscher, P.-A. Malmqvist, L. SerranoAndres, K. Pierloot, M. Merchán, Advances in chemical physics, vol XCIII **1996**, 93, 219.
[66] M. Pastore, C. Angeli, R. Cimiraglia, Chem. Phys. Lett. **2006**, 422, 522.
[67] B. O. Roos, K. Andersson, M. P. Fülscher, L. Serrano-Andrés, K. Pierloot, M. Merchán, V. Molina, J. Mol. Struct. THEOCHEM **1996**, 388, 257.
[68] I. Fdez. Galván, M. Vacher, A. Alavi, C. Angeli, F. Aquilante, J. Autschbach, J. J. Bao, S. I. Bokarev, N. A. Bogdanov, R. K. Carlson, et al., J. Chem. Theory Comput. **2019**, 15, 5925.
[69] F. Aquilante, J. Autschbach, A. Baiardi, S. Battaglia, V. A. Borin, L. F. Chibotaru, I. Conti, L. De Vico, M. Delcey, I. Fdez. Galván, et al., J. Chem. Phys. **2020**, 152, 214117.
[70] Y. Nishimoto, S. Battaglia, R. Lindh, J. Chem. Theory Comput. **2022**, 18, 4269.

Entry for the Table of Contents

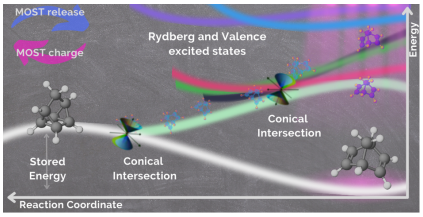

The main photorelaxation pathways regarding the NBD/QC model system have been extensively investigated through high-level ab-initio calculations to shed light on its solar energy storage and release properties. Two strongly coupled reaction coordinates guide and regulate back and forth photoreactivity leading to the formation of conical intersections with different topology that facilitate non-adiabatic population transfer phenomena. The inclusion of Rydberg excited states and dynamic electronic correlation effects resulted to be crucial for the reliable description of photorelaxation paths at molecular level.